Coherent Atomic and Electronic Heterostructures of Single-Layer MoS_2

Goki Eda,[†,‡,§,*,▽] Takeshi Fujita,[¶,#,*,▽] Hisato Yamaguchi,[⊥] Damien Voiry,[⊥] Mingwei Chen,[¶] and Manish Chhowalla[⊥]

[†]Department of Physics, National University of Singapore, 2 Science Drive 3, Singapore 117542, [‡]Department of Chemistry, National University of Singapore, 3 Science Drive 3, Singapore 117543, [§]Graphene Research Centre, National University of Singapore, 6 Science Drive 2, Singapore 117546, [⊥]Materials Science and Engineering, Rutgers University, 607 Taylor Road, Piscataway, New Jersey 08854, United States , [¶]WPI Advanced Institute for Materials Research, Tohoku University, Sendai 980-8577, Japan, and [#]JST, PRESTO, 4-1-8 Honcho Kawaguchi, Saitama 332-0012, Japan. [▽]These authors contributed equally to this work.

ABSTRACT

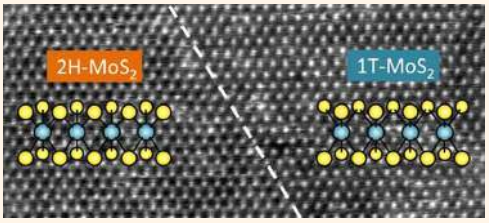

Nanoscale heterostructures with quantum dots, nanowires, and nanosheets have opened up new routes toward advanced functionalities and implementation of novel electronic and photonic devices in reduced dimensions. Coherent and passivated heterointerfaces between electronically dissimilar materials can be typically achieved through composition or doping modulation as in GaAs/AlGaAs and Si/NiSi or heteroepitaxy of lattice matched but chemically distinct compounds. Here we report that single layers of chemically exfoliated MoS_2 consist of electronically dissimilar polymorphs that are lattice matched such that they form chemically homogeneous atomic and electronic heterostructures. High resolution scanning transmission electron microscope (STEM) imaging reveals the coexistence of metallic and semiconducting phases within the chemically homogeneous two-dimensional (2D) MoS_2 nanosheets. These results suggest potential for exploiting molecular scale electronic device designs in atomically thin 2D layers.

KEYWORDS: MoS_2 · 2D crystals · electron microscopy · heterostrucure · interface

Heterostructures of semiconductors and metals form fundamental building blocks of modern electronic and photonic devices.[1] Atomically sharp, coherent and passivated interfaces in such heterostructures are particularly important in high mobility transistors, solid state lasers, light emitting devices, and solar cells where the performance is limited by interfacial defects. Implementation of heterostructures in low dimensional structures such as quantum dots,[2] nanowires,[3] and nanosheets[4] is thus a key step toward enabling their integration into novel nanoscale devices. Single crystal heterostructures are typically realized with chemically dissimilar lattice-matched compounds *via* heteroepitaxy or solid-state reactions. For example, silicon forms coherent interface with metallic nickel silicide (NiSi) such that when Si nanowires are reacted with Ni, metal-semiconductor heterojunctions are achieved.[5] Similarly, a lattice match of graphene and hexagonal boron nitride (hBN) enables hybrid structures in two dimensions.[4] The atomically thin 2D sheet of molybdenum disulfide (MoS_2) is unique in that it is chemically homogeneous but exhibits semiconducting and metallic polymorphs that are lattice matched. Here, we report that chemically exfoliated MoS_2 single layers exhibit a hybrid structure of semiconducting and metallic phases that are coherently bonded such that the resulting single-layer heterostructure is chemically monolithic and single crystalline.

A single layer of molybdenum disulfide (SL-MoS_2) consists of a 6.7 Å thick slab of a S−Mo−S sandwich layer.[6] Recent reports on direct band gap photoluminescence properties,[7−9] field effect transistor characteristics,[10] gas sensitivity,[11] and mechanical stability[12,13] of SL-MoS_2 have opened up new prospects for the technological applications of 2D materials derived from layered inorganic compounds. Polymorphism is one of the unique features of layered transition metal dichalcogenides. MoS_2 and WS_2 exist in both metallic and semiconducting phases. Our previous studies indicate that two phases coexist in chemically exfoliated sheets of MoS_2 and WS_2 (ref 14) pointing to the electronic heterostructural nature which may be exploited for realization of novel nanodevices with advanced functionalities.

Solution-based exfoliation of graphite and inorganic layered compounds has been demonstrated to be a versatile route to the

* Address correspondence to g.eda@nus.edu.sg, tfujita@wpi-aimr.tohoku.ac.jp.

Received for review June 1, 2012 and accepted July 16, 2012.

Published online July 16, 2012
10.1021/nn302422x

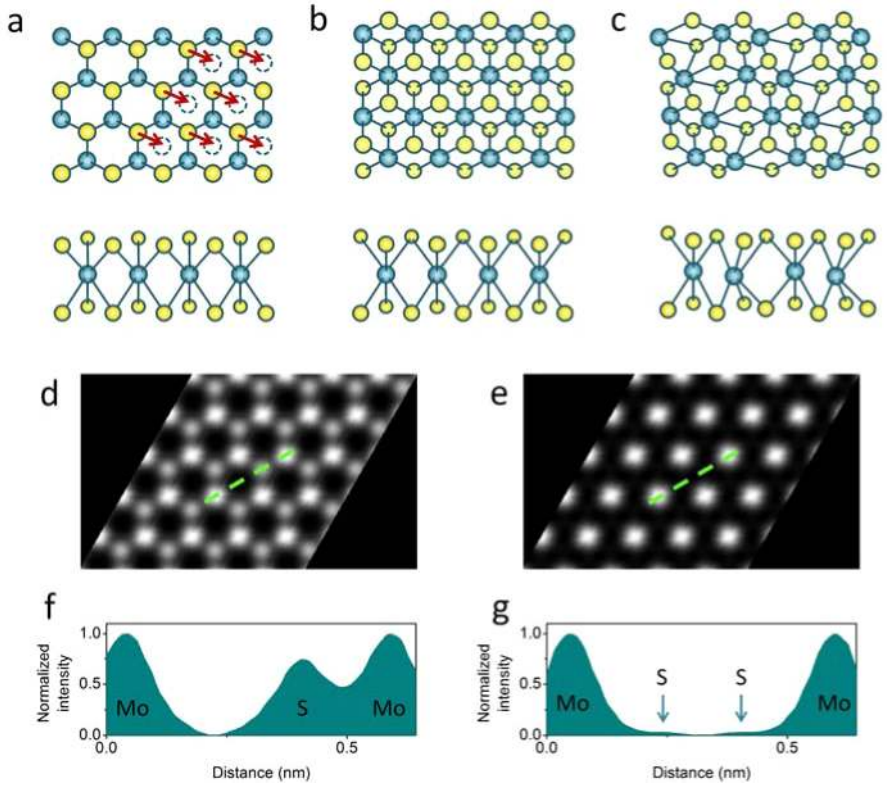

Figure 1. Schematic illustration of the structure of (a) 2H, (b) 1T, and (c) 1T′ phases viewed from the out-of-plane and in-plane axes. The blue and yellow balls represent Mo and S atoms. For the 2H phase (a), only the S atoms on the upper planes can be seen from the *c*-axis as those on the lower planes are directly beneath. The arrows in panel a show the local S plane glide motion that leads to local transformation to 1T structure. (d, e) Simulated HAADF STEM images of ideal (d) 2H and (e) 1T phases. The bright spots correspond to Mo atoms. In the 2H phase, S atoms are visible as less bright spots. (f, g) Intensity profile along the lines indicated in images d and e are shown in images f and g, respectively.

bulk production of 2D sheets and could be a viable method for implementation into technology.[15,16] Ultrasonication of the bulk material in an appropriate organic solvent has also been reported as a simple approach to exfoliation for a number of layered compounds.[16] The yield of single layers is typically low, but the crystal structure of the exfoliated layers remains undisturbed during the process.

Layered transition metal dichalcogenides can be efficiently exfoliated *via* lithium intercalation and subsequent addition of excess water which leads to hydrogen formation and forced separation of the layers.[17,18] This process results in exfoliated layers in a metastable phase.[19] For the case of MoS_2 and WS_2, electron transfer from Li during intercalation causes a change in the electron count from d^2 to d^3, leading to destabilization of the original crystal structure.[20] Specifically, Li intercalation results in a change in the metal coordination from trigonal prismatic (2H) to octahedral geometry (1T).[21] The 1T phase is metastable and persists after exfoliation and removal of Li until it is subject to heating or aging.[22] The two phases exhibit substantially different electronic structures due to the changes in the crystal symmetry. 2H-MoS_2 is a semiconductor with a band gap between the filled d_z^2 and empty $d_{x^2-y^2,xy}$ bands while the 1T phase is metallic with Fermi level lying in the middle of degenerate $d_{xy,yz,xz}$ single band.[23] We recently demonstrated that SL-MoS_2 obtained *via* Li intercalation exhibits a mixed phase structure and that the phase composition strongly influences the electronic properties of the material.[14]

Our studies indicate that chemically exfoliated SL-MoS_2 exhibits a biphase structure with semiconducting and metallic regions. While a number of reports discuss the structural distortion induced during Li intercalation,[19,22,24−26] the biphase nature and its influence on the physical characteristics of the material remains unexplored. Here, we report high resolution scanning transmission electron microscopy (STEM) imaging of chemically exfoliated SL-MoS_2. We demonstrate direct observation of the heterogeneous phase structure consisting of both 2H and 1T phases. Our observations reveal that the structure is highly inhomogeneous consisting of nanometer-sized domains of each phase as well as other regions where the lattice is strongly distorted due to clusterization of the metal atoms.

High resolution scanning TEM (STEM) has proven to be an extremely powerful tool in revealing the atomic structure of 2D materials. In particular high angle annular dark-field (HAADF) imaging mode allows investigation of atomic arrangement in the thickness

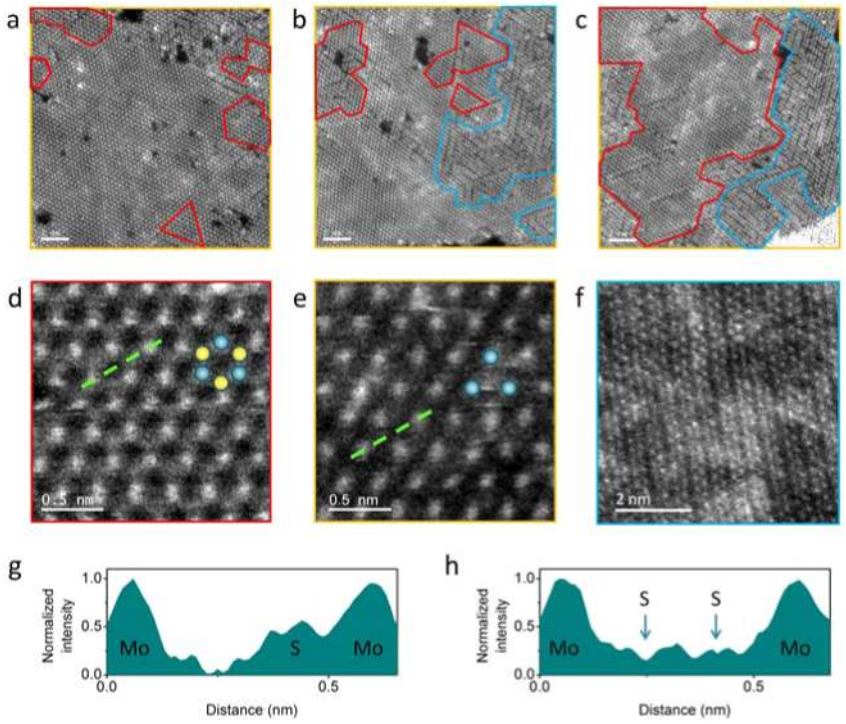

Figure 2. (a–c) STEM images of various regions of chemically exfoliated SL-MoS_2. Regions of 2H, 1T, and 1T′ phases are enclosed by red, yellow, and blue lines. In images a and b, domains of 2H structures are observed in a region which is predominantly in the 1T phase. The scale bars are 2 nm. (d–f) High resolution STEM images of (d) 2H, (e) 1T, and (f) 1T′ phases. The blue and yellow balls in image d and e indicate the position of Mo and S atoms. (g, h) Intensity profiles along the lines indicated in images d and e are shown in images g and h, respectively.

direction due to Z-contrast, which can be used for the identification of single layers[16] and atomic scale edge structure.[27] In this study, we utilize the Z-contrast in HAADF STEM to identify regions with different structures and their distribution over the 2D sheet.

RESULTS/DISCUSSION

An individual layer of MoS_2 consists of a slab of hexagonal Mo lattice sandwiched between two layers of hexagonally packed S. In 2H structure, the stacking sequence is BaB AbA, where capital and lower case letters denote S and Mo atoms, respectively. The coordination of Mo with S in 2H-MoS_2 is trigonal prismatic and the S atoms in the upper layer are located directly above those on the lower layer as schematically shown in Figure 1a. On the other hand, the stacking sequence for 1T-MoS_2 is AbC where S atoms in the upper and lower planes are offset from each other and the Mo atoms occupy the octahedral holes of the S layers as shown in Figure 1b. It can be seen that 2H to 1T transformation can be realized by gliding one of the S planes in the $\langle 2100 \rangle$ direction by $a/\sqrt{3}$. Figure 1a shows an example of local S plane glide motion that leads to creation of the 2H-1T interface.

Chemically exfoliated MoS_2 is in metastable 1T phase and is also substantially distorted, deviating from the ideal 1T structure.[22,26] Studies have indicated that the distorted 1T phase, denoted here as 1T′, exhibits superlattice structure resulting from clusterization of Mo atoms into zigzag chains (Figure 1c) according to previous diffraction, X-ray absorption spectroscopy,[22,26] and scanning tunnelling microscope studies.[24] The displacement of atoms from the equilibrium hexagonal lattice sites also results in departure from full planarity.[25]

Owing to the different atomic arrangements of 2H, 1T, and the 1T′ structures, their direct identification is possible with HAADF STEM imaging. Figure 1 panels d and e show simulated HAADF STEM images of 2H and 1T MoS_2 single layers, respectively. The variations in the signal intensity show clear difference for the two structures. For 2H-MoS_2, the signal from the S sites are enhanced due to overlap of two sulfur atoms along the electron beam direction, making the contrast almost comparable to that of Mo sites despite the lower atomic number (Z).[28] On the other hand, S atoms in the 1T-MoS_2 single layer are evenly distributed around the Mo sites resulting in strong contrast between the Mo and S sites. According to our simulations (Figure 1d,e), the intensity ratio between 2S and Mo sites are found to be 0.74 and 0.03 for 2H and 1T phases, respectively. Thus, honeycomb lattice intensity variation with minor contrast between two adjacent sites is a signature of the 2H-MoS_2 single layer, whereas the hexagonal lattice is a signature of the 1T structure.

Figure 2 panels a–c show high resolution HAADF STEM images of various regions of chemically exfoliated SL-MoS_2 sheets. Crystalline order can be clearly observed despite the presence of vacancy defects.

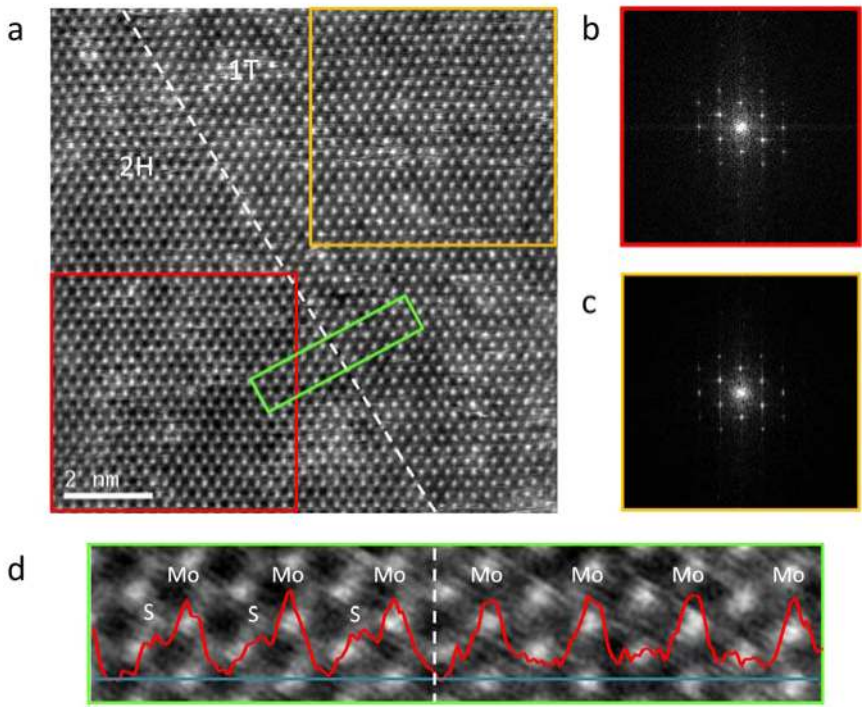

Figure 3. (a) STEM image of a region where a boundary between 2H (left) and 1T (right) phases is observed. The phase boundary is parallel to {-1100} planes and marked by a dashed line. (b, c) Fourier transform image of the (b) lower left and (c) upper right box of the STEM images. (d) Enlarged image of the region indicated by the green rectangle in image a. The intensity profile along the blue line is overlaid on the image. The width of the image corresponds to 3.9 nm.

It should be mentioned that some of the vacancy defects were formed during imaging due to high electron beam energy (120 keV) which is larger than the knock-on energy for MoS_2.[27] Careful examination of the STEM images reveals that the MoS_2 sheets consist of structurally distinct domains. Honeycomb lattice intensity variations consistent with the simulated 2H-MoS_2 single layers were observed in various regions of the samples (Figure 2d). A predominant fraction of the as-exfoliated sheets exhibited hexagonal intensity variations in agreement with the simulated STEM image for 1T-MoS_2 single layer (Figure 2e). Typical intensity ratios between the 2S and Mo sites were found to be 0.6−0.7 and <0.3 for the 2H and 1T regions, respectively, in reasonable agreement with the simulation (Figure 2g,h). The deviation from simulation results can be readily explained by the effect of thermal vibrations and the presence of surface contaminations. These observations demonstrate that the chemically exfoliated MoS_2 is highly heterogeneous in structure consisting of 1T and 2H domains which are typically at least a few nanometers in size.

In addition to 1T and 2H phases, our STEM images also reveal the existence of distorted 1T′ structure consisting of Mo zigzag chains in agreement with the previous studies.[26,29] Interestingly, the orientation and the length of the zigzag chains are not uniform throughout individual sheets. Each chain is either disrupted by another chain or is merged with another chain *via* 60° or 120° kinks, resulting in overall maze-like structure (Figure 2b,c). Although the chain orientations were typically random with short coherence lengths (<5 nm), ordered arrays of zigzag chains were also observed as shown in Figure 2f. The structure of such ordered regions can be described by a $2a \times a$ superlattice in agreement with previous observations.[24,26]

It is worth noting that the zigzag chains were unstable under electron beam exposure and relaxed to 1T structure during imaging. This suggests that the zigzag chain clusters are only formed on the 1T phase rather than on 2H phase. An electron beam did not induce further transformation from the 1T to 2H phase, suggesting that the activation barrier for the phase transformation is greater than the relaxation of the zigzag chain distortion. From earlier studies, it was believed that the 2H to 1T phase transformation during intercalation is always accompanied by lattice distortion.[26] We observed that the distorted 1T′ phase can be relaxed to the undistorted 1T phase with electron beam irradiation without fully transforming it to the 2H phase. Our observation indicates that transformation from 1T′ to 2H phase is a multistep process which goes through an intermediate metastable 1T phase and that similar 1T′ to 1T relaxation may be induced by other means such as mild heating. The activation energy for 1T to 2H phase transition in WS_2 was previously measured to be 0.85 eV/atom.[30] It is known that the 1T phase of WS_2 is more stable than that of MoS_2.

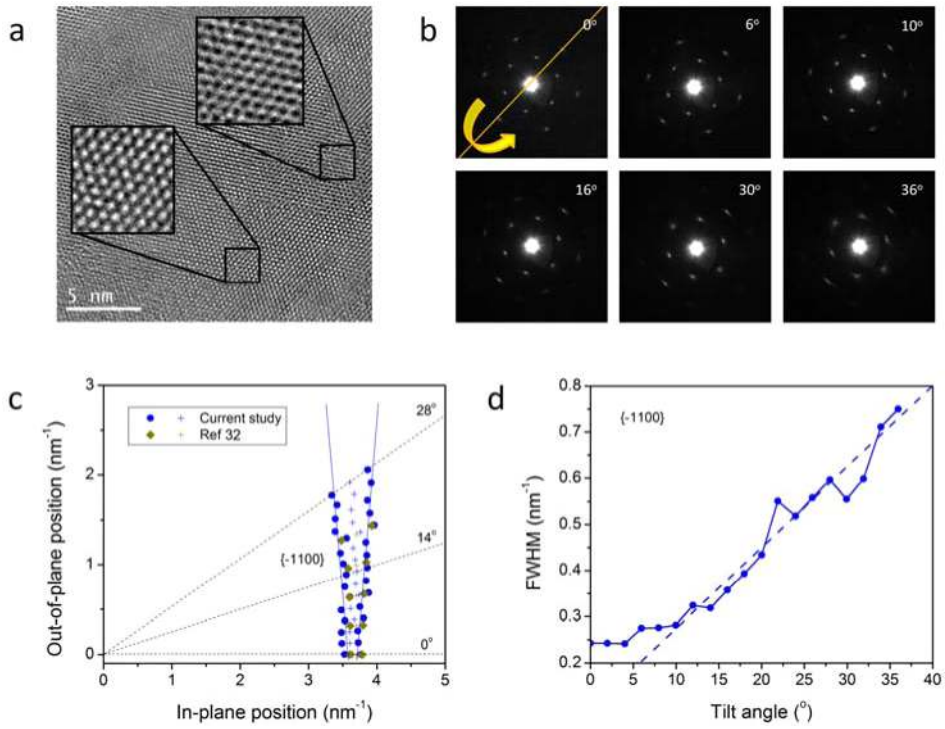

Figure 4. (a) High resolution bright-field TEM image of SL-MoS_2. Two regions indicated by squares are enlarged to show the reversed contrast. (b) SAED patterns of SL-MoS_2 at different tilt angles. The rotation axis is indicated in the 0° tilt image. (c) Reciprocal space representation of the cone formed by relrods due to corrugation of the MoS_2 sheet. The peak centers and fwhm obtained from the $\{-1100\}$ SAED spot are marked by crosses and solid circles, respectively. For comparison, previously reported data for mechanically exfoliated SL-MoS_2 from ref 32 is also shown. (d) The fwhm as a function of tilt angle for the $\{-1100\}$ peak. A linear fit of the plot is shown as the dashed line. The first four points which are largely due to the inherent probe beam diameter are discounted for the linear fit.

Thus relaxation of the 1T′ structure in MoS_2 is expected to require energy significantly smaller than 0.85 eV/atom. It may also be noted that the energy difference (ΔE) between the 1T and 2H phases of MoS_2 has been calculated to be 0.27 eV/atom.[31]

The boundary of two phases was observed to typically occur along the crystal direction. Figure 3a shows the boundary region between the 1T and 2H phases. The hexagonal arrangement of Mo and its orientation remains undisturbed across the boundary as confirmed by the nearly identical Fourier Transform image of the two phases (Figure 3b,c). The difference in the lattice constants of the two regions could not be resolved indicating that the phase boundary is largely strain-free despite the nonideal coordination of the Mo atoms at the interface region. The intensity profile across the boundary in Figure 3d shows sudden change where alternate S−Mo peaks are observed on the 2H phase side and only Mo peaks are observed on the 1T side demonstrating the atomically abrupt interface.

In our recent XPS study we observed two distinct sets of Mo3d and S2p peaks which we assigned to 2H and 1T-type phases.[14] We found that relative fraction of the 1T-type component diminished with increasing annealing temperature from ~0.5 for as-exfoliated material to <0.1 for samples annealed at 300 °C. Here, we examined the structures from randomly chosen areas in a total of ~5,000 nm^2 and found that there is approximately equal amounts of 2H and 1T-type phases in the as-exfoliated samples in agreement with the XPS analysis. However, from a similar survey of phase content in the samples that were annealed at 100, 200, and 300 °C (not shown in the figures), no clear trend in the phase fraction change could be identified within the volume of the samples investigated. Instead, the observable trend was fewer 1T′ phases for a higher annealing temperature. Our STEM observation suggested that an appreciable amount (>0.1) of 1T phase resides in the 300 °C sample, while the 1T′ phase is nearly absent. The presence of 1T phase residues suggests that they are stabilized due to defects or electron donating surface adsorbates.[31] While further statistical analysis is needed for conclusive quantitative analysis, these preliminary results suggest that the set of Mo3d and S2p peaks that we previously assigned to 1T-type phase primarily arise from the 1T′ component. Thus simplified analysis of the XPS results may lead to an underestimation of the fraction of residual 1T phase. These new findings prompt the need for refining the evaluation of the phase components by XPS.

It was recently shown[32] that a suspended sheet of SL-MoS_2 exhibits intrinsic ripples similar to that of graphene.[33] The height of the ripples was estimated

to be on the order of 1 nm for both MoS_2 and graphene. Ripples in the 2D layers are expected to play an important role in the stabilization of the structure as well as charge transport across the sheet.[34] Ripple structure in chemically exfoliated MoS_2 may be influenced by distortion due to clusterization of Mo atoms and the presence of phase boundaries. Figure 4a shows a high resolution TEM image of a single-layer sheet. It can be seen that the contrast fluctuates over a distance of a few nanometers, suggesting the presence of ripples with a length scale of similar magnitude. The reciprocal lattice space of corrugated sheet consists of a cone-shaped volume where the cone angle scales with the magnitude of undulations, or deviation of the surface normal from the mean. The electron diffraction spot becomes consistently blurred as the electron beam deviates from the surface normal (Figure 4b). The corrugation of a suspended 2D sheet can be quantitatively evaluated by studying the width of electron diffraction spots as a function of the tilt angle. Figure 4c shows the plot of peak center and full width at half maxima (fwhm) in the reciprocal space for the $\{-1100\}$ reflections. The data for mechanically exfoliated MoS_2 from ref 32 are also plotted for comparison. The cone angles were found to vary between 8−13°, comparable to the values reported for the mechanically exfoliated sheets. Linear increase of the fwhm with tilt angle suggests uniform ripple structures across the probed regions (Figure 4d). The slope of the curve is on a similar order of magnitude as that in the case of mechanically exfoliated MoS_2 and graphene. The corrugation height is thus estimated to be around 1 nm. Thus our results indicate that the microscopic ripple structure of the sheets is not affected by the structural distortion in the atomic scale, heterogeneous phase structure, and high local pressure involved in the forced exfoliation of Li_xMoS_2.

CONCLUSION

Our STEM observations reveal that a 2D MoS_2 sheet consists of nanometer-sized domains of semiconducting 2H and metallic 1T phases that form coherent interfaces with each other. Local distortions due to clusterization of Mo atoms are also identified in the 1T phase. We also show that the microscopic ripple structure of chemically exfoliated SL-MoS_2 is comparable to that of mechanically exfoliated counterparts despite the structural inhomogeneities. The two polymorphs of SL-MoS_2 which allow formation of coherent electronic heterostructures represent a unique characteristic of the material that may be exploited for novel molecular functionalities.

METHOD

A colloidal suspension of SL-MoS_2 was prepared and the particles were deposited on a TEM grid using the previously reported transfer method.[14] Both as-deposited and annealed samples were observed in the STEM. Annealing was conducted in Ar at various temperatures for 1 h. HAADF STEM imaging was performed using JEOL JEM-2100F TEM/STEM with double spherical aberration (Cs) correctors (CEOS GmbH, Heidelberg, Germany). The collecting angle was between 100 and 267 mrad. The lens aberrations were optimized by evaluating the Zemlin tableau of amorphous carbon. The residual spherical aberration was almost zero ($C_s = -0.8 \pm 1.2\,\mu$m with 95% certification). The acceleration voltage was set to 120 kV which is the lowest voltage with effective C_s correctors in the system. SL-MoS_2 was identified by observing the STEM signal intensity of individual lattice sites as described in the previous reports. Occasionally, beam-induced damage occurred during observation resulting in the formation of point defects and vacancy clusters. Thus the observation time was minimized to avoid beam-induced changes. The HAADF STEM simulations were performed using the xHREM software (HREM Research). The algorithm of the code has been verified to be reliable for simulating C_s-corrected STEM images.[35] In the calculations, the probe convergence angle is 25 mrad and the HAADF detector inner and outer angles are 100 and 267 mrad, respectively.

Conflict of Interest: The authors declare no competing financial interest.

Acknowledgment. G.E. acknowledges the Singapore National Research Foundation for funding the research under the NRF Research Fellowship. G.E. also acknowledges the Royal Society for the Newton International Fellowship and financial support from the Centre for Advanced Structural Ceramics (CASC) at Imperial College London. M.C. and D.V. acknowledge support from NSF ECCS Award 1128335. H.Y. acknowledges the Japan Society for the Promotion of Science (JSPS) for financial support through Postdoctoral Fellowship for Research Abroad. This research was partly supported by JST, PRESTO, and JSPS, Grant-in-Aid for challenging Exploratory Research (24656028).

REFERENCES AND NOTES

1. Sze, S. *Physics of Semiconductor Devices*; Wiley-Interscience: New York, 1981.
2. Dabbousi, B. O.; RodriguezViejo, J.; Mikulec, F. V.; Heine, J. R.; Mattoussi, H.; Ober, R.; Jensen, K. F.; Bawendi, M. G. (CdSe)ZnS Core−Shell Quantum Dots: Synthesis and Characterization of a Size Series of Highly Luminescent Nanocrystallites. *J. Phys. Chem. B* **1997**, *101*, 9463–9475.
3. Lauhon, L. J.; Gudiksen, M. S.; Wang, D.; Lieber, C. M. Epitaxial Core−Shell and Core−Multishell Nanowire Heterostructures. *Nature* **2002**, *420*, 57–61.
4. Ci, L.; Song, L.; Jin, C.; Jariwala, D.; Wu, D.; Li, Y.; Srivastava, A.; Wang, Z. F.; Storr, K.; Balicas, L.; *et al.* Atomic Layers of Hybridized Boron Nitride and Graphene Domains. *Nat. Mater.* **2010**, *9*, 430–435.
5. Wu, Y.; Xiang, J.; Yang, C.; Lu, W.; Lieber, C. M. Single-Crystal Metallic Nanowires and Metal/Semiconductor Nanowire Heterostructures. *Nature* **2004**, *430*, 61–65.
6. Novoselov, K. S.; Jiang, D.; Schedin, F.; Booth, T. J.; Khotkevich, V. V.; Morozov, S. V.; Geim, A. K. Two-Dimensional Atomic Crystals. *Proc. Nat. Acad. Sci. U.S.A.* **2005**, *102*, 10451–10453.
7. Li, T.; Galli, G. Electronic Properties of MoS_2 Nanoparticles. *J. Phys. Chem. C* **2007**, *111*, 16192–16196.
8. Mak, K. F.; Lee, C.; Hone, J.; Shan, J.; Heinz, T. F. Atomically Thin MoS_2: A New Direct-Gap Semiconductor. *Phys. Rev. Lett.* **2010**, *105*, 136805.
9. Splendiani, A.; Sun, L.; Zhang, Y.; Li, T.; Kim, J.; Chim, C.-Y.; Galli, G.; Wang, F. Emerging Photoluminescence in Monolayer MoS_2. *Nano Lett.* **2010**, *10*, 1271–1275.

10. Radisavljevic, B.; Radenovic, A.; Brivio, J.; Giacometti, V.; Kis, A. Single-Layer MoS_2 Transistors. *Nat. Nanotechnol.* **2011**, *6*, 147–150.
11. Li, H.; Yin, Z.; He, Q.; Li, H.; Huang, X.; Lu, G.; Fam, D. W. H.; Tok, A. I. Y.; Zhang, Q.; Zhang, H. Fabrication of Single- and Multilayer MoS_2 Film-Based Field-Effect Transistors for Sensing NO at Room Temperature. *Small* **2012**, *8*, 63–67.
12. Radisavljevic, B.; Whitwick, M. B.; Kis, A. Integrated Circuits and Logic Operations Based on Single-Layer MoS_2. *ACS Nano* **2011**, *5*, 9934–9938.
13. Bertolazzi, S.; Brivio, J.; Kis, A. Stretching and Breaking of Ultrathin MoS_2. *ACS Nano* **2011**, *5*, 9703–9709.
14. Eda, G.; Yamaguchi, H.; Voiry, D.; Fujita, T.; Chen, M.; Chhowalla, M. Photoluminescence from Chemically Exfoliated MoS_2. *Nano Lett.* **2011**, *11*, 5111–5116.
15. Hernandez, Y.; Nicolosi, V.; Lotya, M.; Blighe, F. M.; Sun, Z.; De, S.; McGovern, I. T.; Holland, B.; Byrne, M.; Gun'Ko, Y. K.; *et al*. High-Yield Production of Graphene by Liquid-Phase Exfoliation of Graphite. *Nat. Nanotechnol.* **2008**, *3*, 563–568.
16. Coleman, J. N.; Lotya, M.; O'Neill, A.; Bergin, S. D.; King, P. J.; Khan, U.; Young, K.; Gaucher, A.; De, S.; Smith, R. J.; *et al*. Two-Dimensional Nanosheets Produced by Liquid Exfoliation of Layered Materials. *Science* **2011**, *331*, 568–571.
17. Joensen, P.; Frindt, R. F.; Morrison, S. R. Single-Layer MoS_2. *Mater. Res. Bull.* **1986**, *21*, 457–461.
18. Yang, D.; Frindt, R. F. Li-Intercalation and Exfoliation of Ws_2. *J. Phys. Chem. Solids* **1996**, *57*, 1113–1116.
19. Sandoval, S. J.; Yang, D.; Frindt, R. F.; Irwin, J. C. Raman-Study and Lattice-Dynamics of Single Molecular Layers of MoS_2. *Phys. Rev. B* **1991**, *44*, 3955–3962.
20. Kertesz, M.; Hoffmann, R. Octahedral *vs* Trigonal-Prismatic Coordination and Clustering in Transition-Metal Dichalcogenides. *J. Am. Chem. Soc.* **1984**, *106*, 3453–3460.
21. Py, M. A.; Haering, R. R. Structural Destabilization Induced by Lithium Intercalation in MoS_2 and Related-Compounds. *Can. J. Phys.* **1983**, *61*, 76–84.
22. Yang, D.; Sandoval, S. J.; Divigalpitiya, W. M. R.; Irwin, J. C.; Frindt, R. F. Structure of Single-Molecular-Layer MoS_2. *Phys. Rev. B* **1991**, *43*, 12053–12056.
23. Mattheis., Lf Band Structures of Transition-Metal-Dichalcogenide Layer Compounds. *Phys. Rev. B* **1973**, *8*, 3719–3740.
24. Qin, X. R.; Yang, D.; Frindt, R. F.; Irwin, J. C. Real-Space Imaging of Single-Layer MoS_2 by Scanning Tunneling Microscopy. *Phys. Rev. B* **1991**, *44*, 3490–3493.
25. Prouzet, E.; Heising, J.; Kanatzidis, M. G. Structure of Restacked and Pillared WS_2: An X-ray Absorption Study. *Chem. Mater.* **2002**, *15*, 412–418.
26. Heising, J.; Kanatzidis, M. G. Structure of Restacked MoS_2 and WS_2 Elucidated by Electron Crystallography. *J. Am. Chem. Soc.* **1999**, *121*, 638–643.
27. Hansen, L. P.; Ramasse, Q. M.; Kisielowski, C.; Brorson, M.; Johnson, E.; Topsøe, H.; Helveg, S. Atomic-Scale Edge Structures on Industrial-Style MoS_2 Nanocatalysts. *Angew. Chem., Int. Ed.* **2011**, *50*, 10153–10156.
28. Hartel, P.; Rose, H.; Dinges, C. Conditions and Reasons for Incoherent Imaging in STEM. *Ultramicroscopy* **1996**, *63*, 93–114.
29. Qin, X. R.; Yang, D.; Frindt, R. F.; Irwin, J. C. Scanning Tunneling Microscopy of Single-Layer MoS_2 in Water and Butanol. *Ultramicroscopy* **1992**, *44*−*42*, 630–636.
30. Tsai, H.-L.; Heising, J.; Schindler, J. L.; Kannewurf, C. R.; Kanatzidis, M. G. Exfoliated−Restacked Phase of WS_2. *Chem. Mater.* **1997**, *9*, 879–882.
31. Enyashin, A. N.; Yadgarov, L.; Houben, L.; Popov, I.; Weidenbach, M.; Tenne, R.; Bar-Sadan, M.; Seifert, G. New Route for Stabilization of 1T-WS_2 and MoS_2 Phases. *J. Phys. Chem. C* **2011**, *115*, 24586–24591.
32. Brivio, J.; Alexander, D. T. L.; Kis, A. Ripples and Layers in Ultrathin MoS_2 Membranes. *Nano Lett.* **2011**, *11*, 5148–5153.
33. Meyer, J. C.; Geim, A. K.; Katsnelson, M. I.; Novoselov, K. S.; Booth, T. J.; Roth, S. The Structure of Suspended Graphene Sheets. *Nature* **2007**, *446*, 60–63.
34. Katsnelson, M. I.; Geim, A. K. Electron Scattering on Microscopic Corrugations in Graphene. *Phil. Trans. R. Soc. A* **2008**, *366*, 195–204.
35. Ishizuka, K. A Practical Approach for Stem Image Simulation Based on the FFT Multislice Method. *Ultramicroscopy* **2002**, *90*, 71–83.